Editors' Suggestion | Featured in Physics

Anderson Transition for Light in a Three-Dimensional Random Medium

Alexey Yamilov*
Physics Department, Missouri University of Science & Technology, Rolla, Missouri 65409, USA

Hui Cao†
Department of Applied Physics, Yale University, New Haven, Connecticut 06520, USA

Sergey E. Skipetrov‡
Université Grenoble Alpes, CNRS, LPMMC, 38000 Grenoble, France

(Received 8 August 2024; revised 29 October 2024; accepted 5 December 2024; published 29 January 2025)

We study Anderson transition for light in three dimensions by performing large-scale simulations of electromagnetic wave transport in disordered ensembles of perfect-electric-conducting spatially overlapping spheres. A mobility edge that separates diffusive transport and Anderson localization is identified, revealing a sharp transition from diffusion to localization for light. Critical behavior in the vicinity of the mobility edge is well described by a single-parameter scaling law. The critical exponent is found to be consistent with the value known for the Anderson transition of the orthogonal universality class. Statistical distribution of total transmission at the mobility edge is described without any fit parameter by the diagrammatic perturbation theory originally developed for scalar wave diffusion, but notable deviation from the theory is found when Anderson localization sets in.

DOI: 10.1103/PhysRevLett.134.046302

Anderson localization is a phenomenon of breakdown of quantum or, more generally, wave transport due to interference effects in a disordered medium [1,2]. The existence of Anderson localization has been suggested for electromagnetic waves in general and light in particular [3,4]. Localization of light has indeed been observed in low-dimensional systems [5–9] but not in three dimensions (3D) [10] despite numerous attempts [11–19]. The current belief is that longitudinal electric fields prevent Anderson localization of light in 3D dielectric disordered media [20–23]. Recently, brute-force numerical solutions of Maxwell equations has led to a discovery of light localization [22] in 3D fully disordered ensembles of conducting particles where longitudinal fields either do not exist (in perfect electric conductors) or, at least, are strongly suppressed (in good metals). This finding, however, raises a number of questions: (i) Can the evolution from diffusion to localization of light in conducting disordered systems in Ref. [22] be classified as an Anderson transition? (ii) Is the transition sharp, i.e., does the transition occur at a single frequency that defines a mobility edge? (iii) Does the transition exhibit universal scaling near the mobility edge as predicted by the standard scaling theory of localization [24]? (iv) What is the universality class of this transition for electromagnetic waves? These are the questions that we seek to answer in the present Letter.

*Contact author: yamilov@mst.edu
†Contact author: hui.cao@yale.edu
‡Contact author: sergey.skipetrov@lpmmc.cnrs.fr

Anderson transition has been studied experimentally in various systems, among which electrical (semi-)conductors [25,26] as well as elastic [27,28] and matter [29–32] waves are the most prominent examples. The theory of Anderson transition provides a good understanding of underlying physics [33,34] but lacks quantitative accuracy. This gap is successfully filled by numerical approaches [35–44]. For light, transitions from diffusion to localization and to the photonic band gap regime have been recently studied numerically in 3D disordered photonic band gap materials [45,46].

A sharp transition between extended and localized states is expected only in an infinitely large system, which is impossible to realize experimentally or in numerical simulations. Such difficulty is circumvented by the finite-size scaling approach [47] that investigates how the conductance varies with the system size. The mobility edge separating diffusive transport from Anderson localization is crossed as the energy (frequency ω for light) is varied. On the diffusion side of the mobility edge, the conductance increases with the system size, while on the localization side it decreases as the system gets larger. Moreover, the localization length diverges at the mobility edge ω_c: $\xi(\omega) \propto |\omega - \omega_c|^{-\nu}$. The critical exponent ν depends only on the universality class of the transition, and is independent of any details of particular physical systems.

In this work, we numerically study Anderson transition in 3D fully disordered systems made of metallic scatterers. Compared to experimental studies, numerical calculations

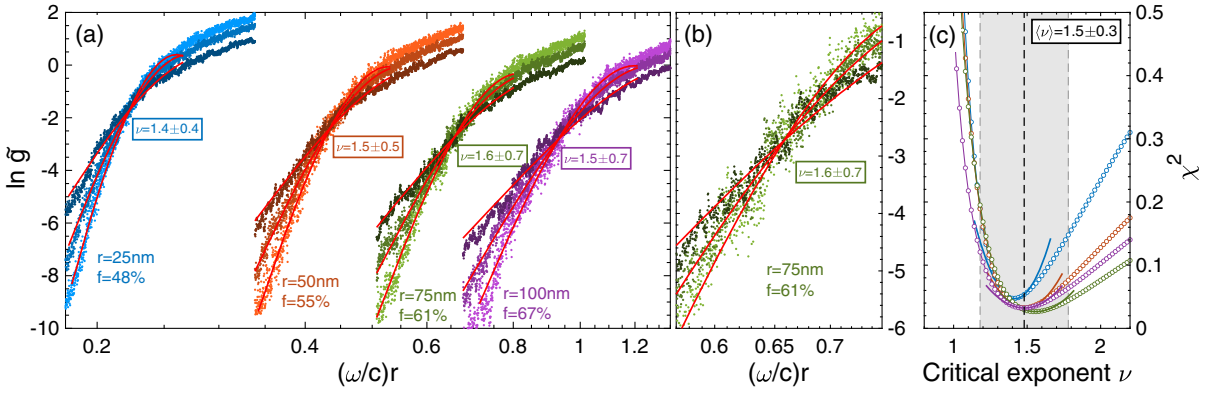

FIG. 1. Transition from diffusion to localization in random ensembles of overlapping spheres. (a) Logarithm of the typical conductance, $\ln \tilde{g}$, as a function of normalized frequency $(\omega/c)r$ for different sphere radii and varying system size $L/\lambda_0 = 3$, 5, and 7 (lighter color for larger L). For a given r, all curves exhibit a crossing. Volume fraction is adjusted to $f = 48\%$, 55%, 61%, and 67% for $r = 25$, 50, 75 and 100 nm (blue, red, green, purple), so that the conductance crossing occurs around $\lambda_0 = 650$ nm for all radii. Solid lines are fits of numerical data to Eq. (2), and the critical exponent ν is given next to each dataset. (b) An expanded view of the crossing point for $r = 75$ nm. (c) χ^2 statistic versus critical exponent ν (symbols), and parabolic fits to the numerical data near minima of χ^2 (solid lines). Estimated uncertainty of ν for each r, given in (a), is obtained from the width of fitted parabola in (c). The mean value of ν and the standard error of the mean are shown in (c) by the vertical dashed line and the shaded area, respectively.

can provide accurate results that are free of experimental artifacts and measurement noises. Moreover, complications from optical absorption may be avoided by simulating perfect-electric-conducting (PEC) materials. Using a highly efficient, hardware-optimized finite-difference time-domain (FDTD) algorithm [48], we directly solve Maxwell equations in space and time for 3D random ensembles of PEC scatterers, see Sec. S1.2 in Ref. [22]. Our numerical results reveal the existence of a mobility edge ω_c for Anderson transition of light, and confirm the single-parameter scaling of the critical behavior in the vicinity of ω_c. We obtain an estimate for the critical exponent $\nu = 1.5 \pm 0.3$, which is consistent with previous results for the Anderson transition in the 3D orthogonal universality class.

To perform the finite-size scaling analysis and to explore the degree of universality of the scaling, we simulate random ensembles of overlapping spheres with four radii r. For each sphere size, we perform time-domain simulation of pulse propagation in a $L \times L \times L$ cube with periodic boundary condition on four sides. The pulse is incident onto the front surface of the cube as a plane wave at normal incidence. The time-dependent transmitted fields are Fourier transformed to obtain the frequency-resolved transmission over a wide spectral range. Then we compute the total transmitted flux at each frequency that, with proper normalization, yields the total transmission $T_a(\omega)$ [48]. Here a denotes the incident spatial mode. Details of numerical simulations are given in Supplemental Material [49] Sec. I.

In principle, the dimensionless conductance can be obtained by summing over input modes a [50,51]: $g = \sum_a T_a$, but simulating all possible input modes a is too resource consuming. Instead, we compute T_a for a single input mode a of linearly polarized plane wave incident normally onto the front surface of the scattering system. Ensemble average over disorder realizations gives $\langle g \rangle = (4/5)N\langle T_a \rangle$, where $N = (\omega L/c)^2/2\pi$ is the number of transverse modes [50,52], and factor 4/5 accounts for angle of incidence, see Supplemental Material [49] Sec. I. Thus, $\langle g \rangle$ can be obtained from $\langle T_a \rangle$, but performing the finite-size scaling of $\langle g \rangle$ would be impractical due to strong fluctuations of T_a from one realization of disorder to another. To circumvent this problem, it is common to work with a typical conductance $\tilde{g}$, which can be, for example, a percentile of the statistical distribution of g or $\exp(\langle \ln g \rangle)$ [38,39]. The precise choice of $\tilde{g}$ has no importance, although some options turn out to be better adapted to numerical evaluation than the others [38]. We choose to average $\ln T_a$ and define

$$\ln \tilde{g} \overset{\text{def}}{=} \langle \ln[(4/5)NT_a] \rangle. \tag{1}$$

Figure 1(a) shows $\ln \tilde{g}$ (dots) versus normalized frequency $(\omega/c)r$ for four sphere radii r and three system sizes L (Table I). Lighter color corresponds to larger L. Statistical averaging is performed over ensembles of 100, 50, and 25 realization for $L/\lambda_0 = 3$, 5 and 7, respectively. For any given r, $\ln \tilde{g}$ increases faster with frequency for larger L. Notably, the conductance curves for different L intersect at a single frequency ω_c. At $\omega < \omega_c$, $\tilde{g}$ decreases with L, a signature of localization. For $\omega > \omega_c$, $\tilde{g}$ increases with L, consistent with diffusion. This indicates a sharp Anderson transition in the $L \to \infty$ limit, with the critical frequency ω_c that can be identified as a mobility edge [24].

We now proceed to the quantitative analysis near the mobility edge ω_c. We employ the following numerically robust procedure for the finite-size scaling analysis [37,39].

TABLE I. Parameters of disordered systems simulated and scaling parameters obtained from fitting for the largest $\Delta\omega_{\rm fit}$.

Radius r (nm)	Filling fraction f	Size L/λ_0	Critical exponent ν	Mobility edge $(\omega_c/c)r$	$\ln\tilde{g}_c$	Critical conductance g_c
25	48%	3, 5, 7	1.4 ± 0.4	$0.22 + 0.01$	-1.7 ± 0.4	0.40 ± 0.01
50	55%	3, 5, 7	1.5 ± 0.5	$0.44 + 0.02$	-2.4 ± 0.6	0.27 ± 0.01
75	61%	3, 5, 7	1.6 ± 0.7	$0.66 + 0.03$	-2.7 ± 0.7	0.23 ± 0.01
100	67%	3, 5, 7	1.5 ± 0.7	$0.93 + 0.05$	-2.8 ± 0.6	0.24 ± 0.01

We fit $\ln\tilde{g}$ datasets corresponding to a given r in a frequency interval $\pm\Delta\omega_{\rm fit}$ around the estimated mobility edge to a scaling function

$$F(\omega, L) = \ln\tilde{g}_c + BL^{1/\nu}(\omega-\omega_c) + CL^{2/\nu}(\omega-\omega_c)^2. \quad (2)$$

Values of the five fit parameters $\ln\tilde{g}_c$, B, C, ω_c and ν are obtained by minimizing the χ^2 statistic defined as

$$\chi^2 = \frac{1}{3}\sum_{i=1}^{3} \frac{1}{N(\Delta\omega_{\rm fit}, L_i)} \sum_{j=1}^{N(\Delta\omega_{\rm fit}, L_i)} \frac{[F(\omega_j, L_i) - \ln\tilde{g}_{ji}]^2}{\sigma_{ji}^2}, \quad (3)$$

where $N(\Delta\omega_{\rm fit}, L_i)$ is the number of data points $(\omega_j, \ln\tilde{g}_{ji})$ in $2\Delta\omega_{\rm fit}$ interval for the system of dimension L_i; $\ln\tilde{g}_{ji}$ is the value of $\ln\tilde{g}$ obtained after ensemble averaging of data at frequency ω_j for the system of size L_i; σ_{ji} is the corresponding standard error of the mean. The fitting results are plotted by solid lines in Fig. 1(a), with an expanded view for $r = 75$ nm in Fig. 1(b). The best-fit parameters ν, ω_c, and $\ln\tilde{g}_c$ are listed in Table I. To obtain their uncertainties, we compute χ^2 as a function of one of them, e.g., ν, with all other parameters fixed at their best-fit values. We then perform a parabolic fit of the dependence $\chi^2(\nu)$ around its minimum at $\nu = \nu_{\rm best}$, see Fig. 1(c), and compute the uncertainty of ν as $\Delta\nu = [2\partial^2\chi^2/\partial\nu^2]^{-1/2}$ at $\nu = \nu_{\rm best}$ [53]. The same analysis is repeated for ω_c and $\ln\tilde{g}_c$; see Supplemental Material [49] Sec. II.

The mobility edge ω_c follows from the fit with a rather small uncertainty and varies very little with $\Delta\omega_{\rm fit}$, see [49] Sec. II. In contrast, the best-fit value of the critical exponent ν varies substantially with $\Delta\omega_{\rm fit}$ but converges robustly towards 1.5 with increasing $\Delta\omega_{\rm fit}$ for all r, see Fig. 2(a). We therefore use the values for the largest $\Delta\omega_{\rm fit}$ for each r as the best estimates of ν. Four systems with different r provide four independent estimates of ν with corresponding uncertainties listed in Table I. Their mean value and the standard error of the mean provide the final estimate for the critical exponent: $\langle\nu\rangle = 1.5 \pm 0.3$. This result is consistent with the value $\nu \simeq 1.57$ previously found for Anderson transition of the orthogonal universality class in various systems: Anderson tight-binding model [37,39], kicked rotor [29,54], random networks of masses connected by springs [43], elastic waves [55], light scattering by cold atoms [56].

The analysis presented above is based on the hypothesis of single-parameter scaling: $\tilde{g} = \tilde{g}(L/\xi)$, where ξ is the localization length. We check to what extent our numerical results are consistent with this hypothesis. This is done by replotting the data of Fig. 1 as a function of the ratio L/ξ, where $\xi = \xi_0/|\omega - \omega_c|^\nu$, in Fig. 3. The unknown constant ξ_0 leads only to a horizontal shift of data points in the chosen logarithmic scale for the horizontal axis. We see that the data points corresponding to different sphere radii [dots in panels (a)–(d)] and different system sizes (colors of different shades) collapse to a single curve given by the scaling function (2) shown by solid lines. This curve has two branches, the top one for diffusion, and the bottom one for localization. Good agreement between our numerical data and the scaling theory confirms that $\tilde{g}$ can be considered as a function of a single parameter L/ξ, and justifies the validity of our analysis *a posteriori*. In Supplemental Material [49] Sec. III, we also test the dependence of our results on the range of system sizes and number of realizations used in the scaling analysis demonstrating the robustness of our analysis.

Our results of single-parameter scaling with similar values of the critical exponent ν for all four different sphere sizes r simulated, as well as the proximity of the values of ν that we find with those from the literature, can be interpreted as a confirmation of the universality of Anderson transition.

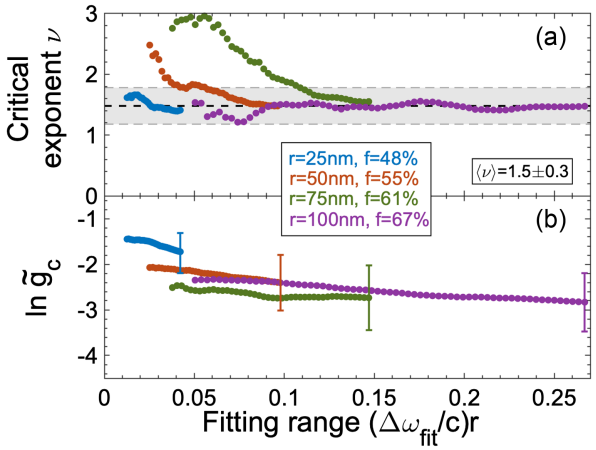

FIG. 2. Critical exponent and typical conductance at the mobility edge. Values of critical exponent ν (a) and of the typical conductance at the mobility edge $\ln\tilde{g}_c$ (b) obtained from fitting in the frequency interval $\pm\Delta\omega_{\rm fit}$ around the estimated mobility edge. In (a), the horizontal dashed line and the shaded gray area show the value of ν averaged over the four sphere radii at the largest internal $\Delta\omega_{\rm fit}$ for reach r and its uncertainty, respectively. In (b), error bars are shown for the largest fitting intervals $\Delta\omega_{\rm fit}$, see Supplemental Material [49] Sec. II.

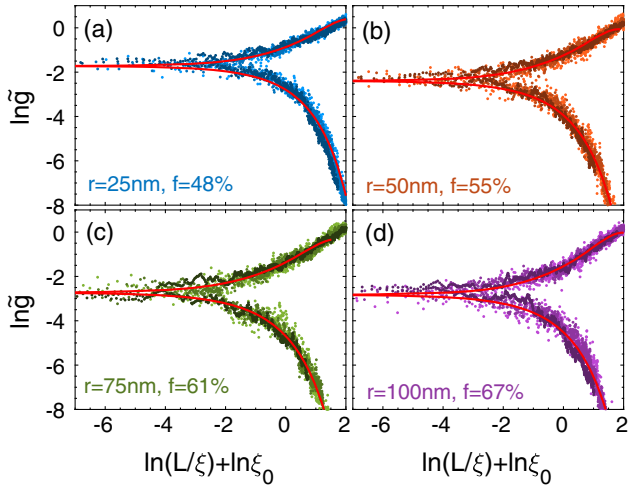

FIG. 3. Numerical data from Fig. 1(a) replotted for each of the four systems in panels (a)–(d) versus system size L normalized by the localization length $\xi = \xi_0/|\omega - \omega_c|^\nu$. All data collapse on universal curves given by the scaling function (2) shown by solid lines, which confirms the validity of the single-parameter scaling hypothesis.

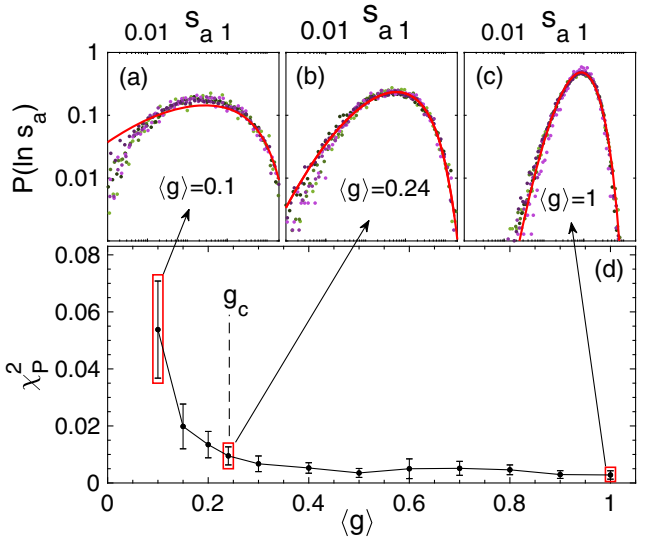

FIG. 4. Statistics of total transmission below, at and above the mobility edge. (a)–(c) Probability density of the normalized transmission $s_a = T_a/\langle T_a\rangle$ for three values of average conductance $\langle g\rangle = 0.1$, 0.24 ($\simeq g_c$), and 1.0, obtained by spectral binning of numerical data for $r = 75$ and 100 nm (with nearly identical g_c) and all system sizes L in Table I (dots). Solid lines show Eq. (4) with the actual values of $\langle g\rangle$. (d) Deviation of Eq. (4) from the numerical $P(s_a)$ as a function of $\langle g\rangle$. The circles and the error bars represent the mean and standard deviation over different r's and L's, respectively.

Namely, the critical behavior is insensitive to microscopic details of disorder as well as to the type of waves and whether they are scalar or vector waves.

The single-parameter scaling shown above relies on the typical conductance $\tilde{g}$ defined in Eq. (1) as the scaling parameter. Since we define $\tilde{g}$ in terms of the total transmission T_a, one may wonder about its relation with the average conductance $\langle g\rangle$, which is believed to be the relevant scaling parameter for the Anderson transition [33]. It is worthwhile to note that even though we compute T_a and not g, we can still obtain the mean $\langle g\rangle = (4/5)N\langle T_a\rangle$ [51]. The value of $\langle g\rangle$ at mobility edge g_c can be estimated by averaging $\langle g\rangle$ over a narrow frequency interval $\delta\omega$ around ω_c. Using $(\delta\omega/c)r = 0.02$ yields g_c that depends only weakly on the range $\Delta\omega_{\rm fit}$ of the fit in Fig. 1. For each sphere size r, averaging over all L's for the largest $\Delta\omega_{\rm fit}$, yields the best estimate for the critical value g_c given in Table I. These values are consistent with the expectation that g_c is of the order of unity [57].

To further illustrate the relation between $\tilde{g}$ in Eq. (1) and $\langle g\rangle$, we study the full probability distribution of T_a. Figures 4(a)–4(c) show the probability density of the normalized transmission $s_a = T_a/\langle T_a\rangle$ for different $\langle g\rangle$, obtained by sampling the ensemble of disorder realizations within different frequency intervals. It is compared to the prediction of the perturbation diagrammatic theory developed for $\langle g\rangle \gg 1$ [58,59] (red solid lines):

$$P(s_a) = \int_{-i\infty}^{i\infty} \frac{dx}{2\pi i} \exp\left[x s_a - \Phi_{\rm con}(x)\right], \tag{4}$$

$$\Phi_{\rm con}(x) = \langle g\rangle \ln^2\left[\sqrt{1 + x/\langle g\rangle} + \sqrt{x/\langle g\rangle}\right]. \tag{5}$$

Figures 4(a)–4(c) show the comparison in three regimes: diffuse transport $\langle g\rangle > g_c$, mobility edge $\langle g\rangle = g_c$, and Anderson localization $\langle g\rangle < g_c$. In Fig. 4(d), we quantify the deviation χ_P^2 between the numerical and theoretical distributions for a given $\langle g\rangle$, see Supplemental Material [49] Sec. II. For $\langle g\rangle \geq g_c$, the agreement between numerical $P(s_a)$ and Eq. (4) is remarkable without any adjustable parameters, with the value of $\langle g\rangle$ that parametrizes $P(s_a)$ calculated directly from $\langle T_a\rangle$ [50]. This not only demonstrates the validity of Eq. (4) for light near and at the localization transition but also, and more importantly, establishes the equivalence of using $\tilde{g}$ or $\langle g\rangle$ as the relevant scaling parameter for the Anderson transition. Indeed, as far as $P(s_a)$ is parametrized only by $\langle g\rangle$—which is the case according to Fig. 4—the average of any function of s_a, including $\ln\tilde{g} \propto \langle \ln s_a\rangle$, is a function of $\langle g\rangle$ and thus can be used as a scaling parameter.

Figure 4 also shows that in the regime of Anderson localization where $\langle g\rangle$ becomes significantly smaller than g_c, Eq. (4) does not hold any more. In particular, the discrepancy between numerical $P(s_a)$ and Eq. (4) is significant for $\langle g\rangle = 0.1$. Even if $\langle g\rangle$ is treated as a fitting parameter, the numerical $P(s_a)$ cannot be satisfactorily fitted by Eq. (4), see Supplemental Material [49] Sec. IV. Nevertheless, the numerical data for different r's and L's in Fig. 4(a) collapse onto a single curve.

Finally, we point out that dissipation is absent in PEC media simulated. Any realistic metal has some degree of optical absorption—an aspect that becomes particularly crucial in the context of Anderson localization [11,12,15]. It would therefore be important to extend the analysis presented in this Letter to disordered media with dissipation. Previous studies have shown that absorption breaks down the single-parameter scaling [60], making it necessary to introduce a second scaling parameter. Finite-size scaling in the framework of two-parameter scaling hypothesis may be an interesting extension of our work for Anderson transition of light in realistic 3D systems.

Acknowledgments—This work is supported partly by the US National Science Foundation (NSF) under Grants No. DMR-1905442, No. DMR-1905465, and by the US Office of Naval Research (ONR) under Grant No. N00014-221-1-2026. We sincerely thank Professor Zongfu Yu and Flexcompute Inc. for providing us access to the Tidy3D software for running all the numerical simulations described in this Letter.

Data availability—The simulation project and the associated code can be found in Ref. [61]. A Tidy3D software license can be requested from Flexcompute Inc to reproduce simulation results.

[1] P. W. Anderson, Absence of diffusion in certain random lattices, Phys. Rev. **109**, 1492 (1958).
[2] B. Kramer and A. MacKinnon, Localization: Theory and experiment, Rep. Prog. Phys. **56**, 1469 (1993).
[3] S. John, Electromagnetic absorption in a disordered medium near a photon mobility edge, Phys. Rev. Lett. **53**, 2169 (1984).
[4] P. W. Anderson, The question of classical localization a theory of white paint?, Philos. Mag. B **52**, 505 (1985).
[5] A. Chabanov, M. Stoytchev, and A. Genack, Statistical signatures of photon localization, Nature (London) **404**, 850 (2000).
[6] Y. Lahini, A. Avidan, F. Pozzi, M. Sorel, R. Morandotti, D. N. Christodoulides, and Y. Silberberg, Anderson localization and nonlinearity in one-dimensional disordered photonic lattices, Phys. Rev. Lett. **100**, 013906 (2008).
[7] T. Schwartz, G. Bartal, S. Fishman, and M. Segev, Transport and Anderson localization in disordered two-dimensional photonic lattices, Nature (London) **446**, 52 (2007).
[8] F. Riboli, P. Barthelemy, S. Vignolini, F. Intonti, A. D. Rossi, S. Combrie, and D. S. Wiersma, Anderson localization of near-visible light in two dimensions, Opt. Lett. **36**, 127 (2011).
[9] M. Segev, Y. Silberberg, and D. N. Christodoulides, Anderson localization of light, Nat. Photonics **7**, 197 (2013).
[10] S. E. Skipetrov and J. H. Page, Red light for Anderson localization, New J. Phys. **18**, 021001 (2016).
[11] D. S. Wiersma, P. Bartolini, A. Lagendijk, and R. Righini, Localization of light in a disordered medium, Nature (London) **390**, 671 (1997).
[12] F. Scheffold, R. Lenke, R. Tweer, and G. Maret, Localization or classical diffusion of light?, Nature (London) **398**, 206 (1999).
[13] D. S. Wiersma, J. G. Rivas, P. Bartolini, A. Lagendijk, and R. Righini, Reply: Localization or classical diffusion of light?, Nature (London) **398**, 207 (1999).
[14] M. Störzer, P. Gross, C. M. Aegerter, and G. Maret, Observation of the critical regime near Anderson localization of light, Phys. Rev. Lett. **96**, 063904 (2006).
[15] T. van der Beek, P. Barthelemy, P. M. Johnson, D. S. Wiersma, and A. Lagendijk, Light transport through disordered layers of dense gallium arsenide submicron particles, Phys. Rev. B **85**, 115401 (2012).
[16] T. Sperling, W. Bührer, C. M. Aegerter, and G. Maret, Direct determination of the transition to localization of light in three dimensions, Nat. Photonics **7**, 48 (2013).
[17] F. Scheffold and D. Wiersma, Inelastic scattering puts in question recent claims of Anderson localization of light, Nat. Photonics **7**, 934 (2013).
[18] G. Maret, T. Sperling, W. Bührer, A. Lubatsch, R. Frank, and C. M. Aegerter, Inelastic scattering puts in question recent claims of Anderson localization of light, Nat. Photonics **7**, 934 (2013).
[19] T. Sperling, L. Schertel, M. Ackermann, G. J. Aubry, C. M. Aegerter, and G. Maret, Can 3D light localization be reached in 'white paint'?, New J. Phys. **18**, 013039 (2016).
[20] S. E. Skipetrov and I. M. Sokolov, Absence of Anderson localization of light in a random ensemble of point scatterers, Phys. Rev. Lett. **112**, 023905 (2014).
[21] B. A. van Tiggelen and S. E. Skipetrov, Longitudinal modes in diffusion and localization of light, Phys. Rev. B **103**, 174204 (2021).
[22] A. Yamilov, S. E. Skipetrov, T. W. Hughes, M. Minkov, Z. Yu, and H. Cao, Anderson localization of electromagnetic waves in three dimensions, Nat. Phys. **19**, 1308 (2023).
[23] T. Micklitz and A. Altland, Topology obstructing Anderson localization of light, arXiv:2405.13277.
[24] E. Abrahams, P. W. Anderson, D. C. Licciardello, and T. V. Ramakrishnan, Scaling theory of localization: Absence of quantum diffusion in two dimensions, Phys. Rev. Lett. **42**, 673 (1979).
[25] T. F. Rosenbaum, K. Andres, G. A. Thomas, and R. N. Bhatt, Sharp metal-insulator transition in a random solid, Phys. Rev. Lett. **45**, 1723 (1980).
[26] M. A. Paalanen, T. F. Rosenbaum, G. A. Thomas, and R. N. Bhatt, Stress tuning of the metal-insulator transition at millikelvin temperatures, Phys. Rev. Lett. **48**, 1284 (1982).
[27] H. Hu, A. Strybulevych, J. H. Page, S. E. Skipetrov, and B. A. van Tiggelen, Localization of ultrasound in a three-dimensional elastic network, Nat. Phys. **4**, 945 (2008).
[28] L. A. Cobus, W. K. Hildebrand, S. E. Skipetrov, B. A. van Tiggelen, and J. H. Page, Transverse confinement of ultrasound through the Anderson transition in three-dimensional mesoglasses, Phys. Rev. B **98**, 214201 (2018).
[29] J. Chabé, G. Lemarié, B. Grémaud, D. Delande, P. Szriftgiser, and J. C. Garreau, Experimental observation of the Anderson metal-insulator transition with atomic matter waves, Phys. Rev. Lett. **101**, 255702 (2008).

[30] S. S. Kondov, W. R. McGehee, J. J. Zirbel, and B. DeMarco, Three-dimensional Anderson localization of ultracold matter, Science **334**, 66 (2011).
[31] F. Jendrzejewski, A. Bernard, K. Müller, P. Cheinet, V. Josse, M. Piraud, L. Pezzé, L. Sanchez-Palencia, A. Aspect, and P. Bouyer, Three-dimensional localization of ultracold atoms in an optical disordered potential, Nat. Phys. **8**, 398 (2012).
[32] G. Semeghini, M. Landini, P. Castilho, S. Roy, G. Spagnolli, A. Trenkwalder, M. Fattori, M. Inguscio, and G. Modugno, Three-dimensional localization of ultracold atoms in an optical disordered potential, Nat. Phys. **11**, 554 (2015).
[33] F. Evers and A. D. Mirlin, Anderson transitions, Rev. Mod. Phys. **80**, 1355 (2008).
[34] P. Wölfle and D. Vollhardt, Self-consistent theory of Anderson localization: General formalism and applications, Int. J. Mod. Phys. B **24**, 1526 (2010).
[35] J. L. Pichard and G. Sarma, Finite size scaling approach to Anderson localisation, J. Phys. C **14**, L127 (1981).
[36] A. MacKinnon and B. Kramer, One-parameter scaling of localization length and conductance in disordered systems, Phys. Rev. Lett. **47**, 1546 (1981).
[37] K. Slevin and T. Ohtsuki, The Anderson transition: Time reversal symmetry and universality, Phys. Rev. Lett. **78**, 4083 (1997).
[38] K. Slevin, P. Markoš, and T. Ohtsuki, Reconciling conductance fluctuations and the scaling theory of localization, Phys. Rev. Lett. **86**, 3594 (2001).
[39] K. Slevin and T. Ohtsuki, Critical exponent for the Anderson transition in the three-dimensional orthogonal universality class, New J. Phys. **16**, 015012 (2014).
[40] D. Delande and G. Orso, Mobility edge for cold atoms in laser speckle potentials, Phys. Rev. Lett. **113**, 060601 (2014).
[41] A. Rodriguez, L. J. Vasquez, K. Slevin, and R. A. Römer, Critical parameters from a generalized multifractal analysis at the Anderson transition, Phys. Rev. Lett. **105**, 046403 (2010).
[42] A. Rodriguez, L. J. Vasquez, K. Slevin, and R. A. Römer, Multifractal finite-size scaling and universality at the Anderson transition, Phys. Rev. B **84**, 134209 (2011).
[43] S. D. Pinski, W. Schirmacher, and R. A. Römer, Anderson universality in a model of disordered phonons, Europhys. Lett. **97**, 16007 (2012).
[44] E. G. Carnio, N. D. M. Hine, and R. A. Römer, Resolution of the exponent puzzle for the Anderson transition in doped semiconductors, Phys. Rev. B **99**, 081201(R) (2019).
[45] J. Haberko, L. S. Froufe-Pérez, and F. Scheffold, Transition from light diffusion to localization in three-dimensional amorphous dielectric networks near the band edge, Nat. Commun. **11**, 4867 (2020).
[46] F. Scheffold, J. Haberko, S. Magkiriadou, and L. S. Froufe-Pérez, Transport through amorphous photonic materials with localization and bandgap regimes, Phys. Rev. Lett. **129**, 157402 (2022).
[47] V. Privman, *Finite Size Scaling and Numerical Simulation of Statistical Systems* (World Scientific, Singapore, 1990).
[48] Flexcompute inc., https://flexcompute.com (accessed: 2024-06-07).
[49] See Supplemental Material at http://link.aps.org/supplemental/10.1103/PhysRevLett.134.046302 for details of numerical simulations and error estimation, tests of robustness of scaling analysis, and statistics of the total transmission in the localized regime.
[50] M. C. van Rossum and T. M. Nieuwenhuizen, Multiple scattering of classical waves: Microscopy, mesoscopy, and diffusion, Rev. Mod. Phys. **71**, 313 (1999).
[51] E. Akkermans and G. Montambaux, *Mesoscopic Physics of Electrons and Photons* (Cambridge University Press, Cambridge, England, 2007).
[52] A. Yamilov, Relation between channel and spatial mesoscopic correlations in volume-disordered waveguides, Phys. Rev. B **78**, 045104 (2008).
[53] P. Bevington and D. Robinson, *Data Reduction and Error Analysis for the Physical Sciences* (McGraw-Hill, New York, 1992).
[54] G. Lemarié, J. Chabé, P. Szriftgiser, J. C. Garreau, B. Grémaud, and D. Delande, Observation of the Anderson metal-insulator transition with atomic matter waves: Theory and experiment, Phys. Rev. A **80**, 043626 (2009).
[55] S. E. Skipetrov and Y. M. Beltukov, Anderson transition for elastic waves in three dimensions, Phys. Rev. B **98**, 064206 (2018).
[56] S. E. Skipetrov, Localization transition for light scattering by cold atoms in an external magnetic field, Phys. Rev. Lett. **121**, 093601 (2018).
[57] A. Mirlin, Statistics of energy levels and eigen-functions in disordered systems, Phys. Rep. **326**, 259 (2000).
[58] T. M. Nieuwenhuizen and M. C. W. van Rossum, Intensity distributions of waves transmitted through a multiple scattering medium, Phys. Rev. Lett. **74**, 2674 (1995).
[59] E. Kogan and M. Kaveh, Random-matrix-theory approach to the intensity distributions of waves propagating in a random medium, Phys. Rev. B **52**, R3813 (1995).
[60] L. I. Deych, A. Yamilov, and A. A. Lisyansky, Scaling in one-dimensional localized absorbing systems, Phys. Rev. B **64**, 024201 (2001).
[61] Tidy3D simulation project (2024) https://www.flexcompute.com/tidy3d/q7ras6JBww/.